#### **ORIGINAL RESEARCH ARTICLE**



# Effects of Silver Nanoparticles in Pectin Polysaccharide Thin Film on Resistive Switching Characteristics

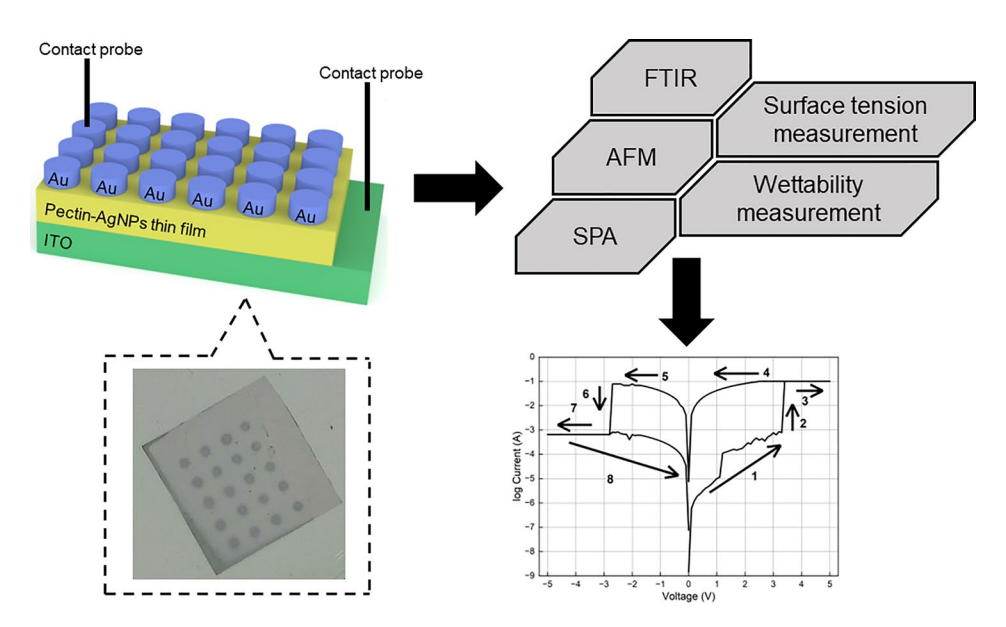
Jia Zheng Yeoh<sup>1</sup> · Muhammad Awais<sup>1</sup> · Feng Zhao<sup>2</sup> · Kuan Yew Cheong<sup>1</sup>

Received: 24 June 2024 / Accepted: 20 August 2024 © The Minerals, Metals & Materials Society 2024

#### Abstract

This study investigates the resistive switching characteristics of Ag nanoparticle (AgNP)-incorporated pectin (pectin-AgNP) as a memristive thin film, with varying concentrations of AgNP (0.0 wt.%, 0.5 wt.%, and 1.0 wt.%) and pectin (5.0 mg/L, 5.5 mg/L, 6.0 mg/L, 6.5 mg/L, and 7.0 mg/L), sandwiched between Au and indium tin oxide (ITO) electrodes on glass substrate. The structural, chemical, and electrical properties of these pectin-AgNP thin films were evaluated. With AgNP concentration of 0.5 wt.% in a pectin concentration of 5.5 mg/mL, the Fourier transform infrared (FTIR) spectra indicated the highest presence of C–O bonds. This suggests the incorporation of AgNP and the formation of more linear and extended pectin chains established by glycosidic bonds. The abundance of C–O bonds contributed significantly to the increase in the resistance of the thin film, consequently yielding the highest ON/OFF ratio (7.2×10³) observed among the samples. The electronic and thermochemical mechanisms governing the resistive switching behaviours were also proposed.

#### **Graphical Abstract**



**Keywords** Pectin · AgNP · resistive switching · C–O bonds · ON/OFF ratio

# Introduction

The evolution of information technology is projected to become more extensive, tailored, and sophisticated as a result of continuous developments in semiconductor devices

Extended author information available on the last page of the article

Published online: 09 September 2024

🖆 Springer

for Internet of Things applications. 1 This has a significant impact on human productivity and lifestyle. Within this context, non-volatile memory (NVM) technologies emerge as a fundamental part of modern information technology to keep pace with this evolution.<sup>2</sup> Among the NVM technologies, resistive switching random access memory (ReRAM) has garnered the most attention due to its simple capacitorlike architecture and fabrication process, large scalability with high data density, fast switching speed, high power efficiency, and cost-effectiveness.<sup>3-5</sup> ReRAM comprises a dielectric active layer sandwiched between two metallic electrodes. This active layer is commonly made of inorganic oxide or fossil-derived polymeric materials.<sup>6,7</sup> It operates based on the principle of reversible switching resistance at a specific voltage, where it exists in two distinct conductivity states and is able to switch between at least two different resistance levels, known as the high-resistance state (HRS, or "OFF") and low-resistance state (LRS, or "ON"), which are equivalent to "0" and "1", respectively, in a binary system.

However, the use of non-renewable materials and disposal of electronic waste (e-waste) pose significant issues of raw material depletion and environmental pollution that directly affects human health. <sup>8,9</sup> According to the Department of Environment Malaysia, it is projected that Malaysians will generate approximately 24.5 million units of e-waste by the year 2025, with this trend expected to continue to steadily increase. The generation of e-waste is an unavoidable consequence of technological expansion. <sup>10,11</sup> To address this challenge, the selection of materials is crucial in developing sustainable electronic devices, such as the consideration of degradability or compatibility with the environment. <sup>12</sup> The integration of bio-organic materials as the active dielectric layer in ReRAM devices could be one such strategy,

as bio-organic materials are abundant in nature, environmentally friendly, and pollution-free. <sup>12,13</sup> In addition, bio-organic materials tend to decompose more rapidly and can be absorbed by microorganisms due to their weaker covalent bonds than those in inorganic materials. This advancement has the potential to significantly enhance the production of sustainable electronic devices while reducing environmental pollution.

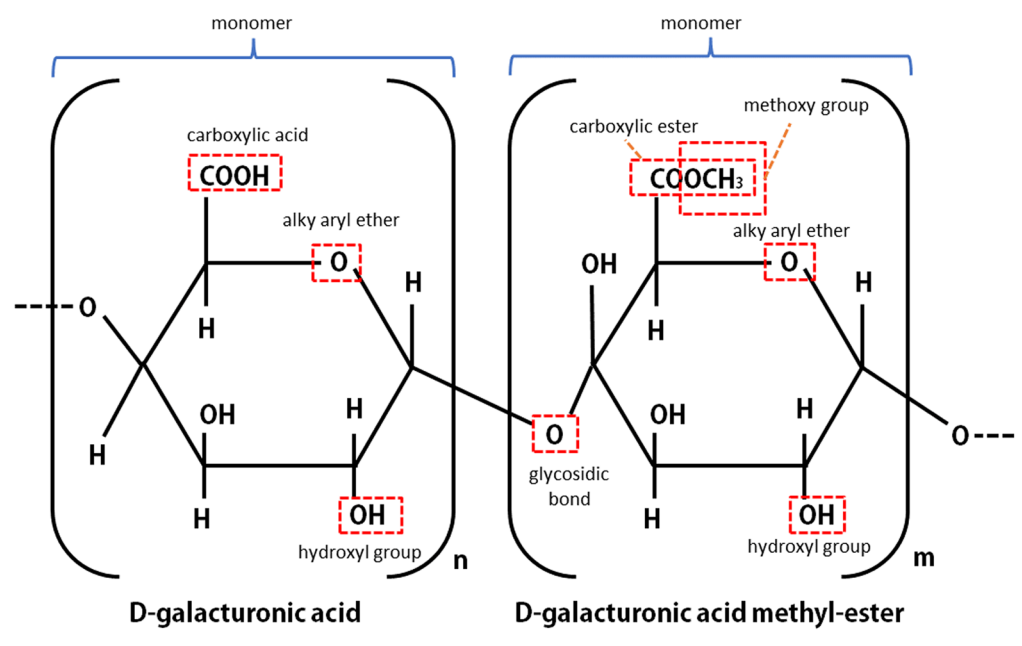
Among a wide range of bio-organic materials, pectin stands out as a promising polysaccharide-based material that offers advantages such as good solubility and rapid transport of metal ions. Table I shows a performance comparison of reported pectin-based ReRAM. Pectin is derived from the primary cell wall of terrestrial plants and fruits such as apples, citrus, and bananas that can be easily obtained from food waste. 14-16 According to Wang et al. 17 and Yap et al., 18 the monomers of pectin are D-galacturonic acid and D-galacturonic acid methyl-ester bonded by  $\alpha$ -(1–4) glycosidic linkages as shown in Fig. 1. The oxygen-containing functional groups in pectin play an important role in interacting with metal ions in the electrode, facilitating the formation of a conductive channel when voltage is applied,<sup>1</sup> which is responsible for resistive switching. Most studies on pectin-based ReRAM materials have reported on two pectin concentration ranges,  $\leq 5$  mg/mL and  $\geq 10$  mg/mL, as shown in Table I. The films with a concentration  $\leq 5$  mg/ mL exhibited a smaller read memory window but a larger ON/OFF ratio relative to films with a concentration > 10 mg/ mL. However, the effects of concentrations ranging between 5 mg/mL and 10 mg/mL on resistive switching performance remain unexplored, and it is one of the main focuses of this study.

Furthermore, as shown in Table I, several studies have demonstrated that the bio-organic dielectric layer with

Pectin-based ReRAM device	Pectin conc. (mg/mL)	$V_{\text{set}}\left(\mathbf{V}\right)$	$V_{\text{reset}}\left(\mathbf{V}\right)$	Read memory window (V)	ON/OFF ratio (10 <sup>n</sup> )	Ref.
Ag/pectin/FTO	33.33, 50, 100	3.3	-4.5	7.5	2	24
Ag/pectin/FTO	NR	1.3	-1.6	2.9	3	25
Ag/pectin/ITO	5	1.0	-0.5	1.5	2	16
Ag/pectin-TiO <sub>2</sub> /FTO	0.02	3	-3	6	5	26
Ag/pectin/FTO	NR	3	-2.8	5.8	4	27
Al/pectin/ITO	0.5, 1.0, 1.5	-2.5	1.75	4.25	4	28
Ag/pectin/ITO	4	3	-3	6	4	18
Al/pectin-AgNO <sub>3</sub> /ITO	2	1.0	-1.2	2.2	3	14
Al/pectin-MoS <sub>2</sub> /ITO	1, 2, 5, 10	1.7	-2	3.7	2	17
Al/pectin-GO/ITO	5	-1.21	2.97	4.18	4	1
Au/pectin-AgNPs/ITO	5.0, 5.5, 6.0, 6.5, 7.0	3.7	-1.8	5.5	3	This work

FTO fluorine-doped tin oxide, GO graphene oxide, NR not reported





Note: n and m refer as number of repeating units  $\geq 1$ 

Fig. 1 Schematic of the chemical structure of pectin monomer and its corresponding functional groups.

additives can significantly enhance the resistive performance of ReRAM. The introduction of additives facilitates the formation of conductive filaments and/or promotes redox reactions, the main conduction mechanism in pectin ReRAM. Among these additives, silver nanoparticle (AgNP) are used extensively in various commercial, industrial, medical, and agricultural applications <sup>19–21</sup> due to their unique electrical and thermal properties.<sup>22</sup> In addition, as reported by Xu et al., 23 AgNP possess good antibacterial and antifungal properties against harmful microorganisms such as Escherichia coli and Staphylococcus aureus. While other noble metals, such as gold and copper, possess similar antibacterial properties, copper is susceptible to oxidation, leading to a reduction in service life, and gold is costly. Hence, silver, as a non-toxic and less costly substance, is the preferred choice for use as an additive in pectin for fabricating ReRAM devices. To the best of our knowledge, so far, only one work has been reported on the use of AgNO<sub>3</sub> instead of AgNP incorporated in the pectin matrix, 14 and the concentration of pectin was lower than 2 mg/mL. In this work, we investigated the structural, chemical, and electrical characteristics of pectin films with a concentration between 5 mg/mL and 10 mg/mL, and with incorporation of AgNP in the pectin matrix to enhance the resistive switching performance. The mechanisms that are responsible for current conduction in pectin-AgNP films are also proposed.

### **Experimental**

Figure 2 shows a schematic of the fabrication procedures for the Au/pectin-AgNP/ITO devices. Commercial pectin powder extracted from citrus peel (galacturonic acid≥74.0 % (dried basis), CAS #9000-69-5, Sigma-Aldrich), AgNP powder (99.95%, 20-30 nm, hermetically sealed, CAS #7440-22-4, SkySpring Nanomaterials, Inc., Houston, TX, USA), and deionized water (UV Water Purification System, Synergy, Milli-Q, Merck Millipore, Germany) were used to prepare the pectin-AgNP precursor solutions. Initially, 5 mg of pectin powder was mixed with three different weights of AgNP powder (0.0 wt.%, 0.5 wt.%, and 1.0 wt.%) in 1 mL of deionized water and stirred until a homogeneous solution was formed. In the meantime, 2 cm × 2 cm ITO-on-glass substrates (sheet resistance 7  $\Omega$ /sq, thickness of 220  $\pm$  30 nm, Zhuhai Kaivo Optoelectronic Technology Co., Ltd, Guangdong, China) were cleaned by sequential immersion for 30 min in ultrasonically agitated baths of acetone (CAS #67-64-1, 95 v/v% (repack), Merck 100014) followed by ethanol (CAS #64-17-5, 95 v/v% (repack), Chemiz 19546) and finally deionized water. Subsequently, 200 µL pectin-AgNP precursor solution was drop-cast onto the cleaned and dried ITOon-glass substrate using a micropipette (Pipetman Classic P1000, Gilson, Middleton, WI, USA). The samples were then baked in an oven (UFB 400, Memmert, Germany) at



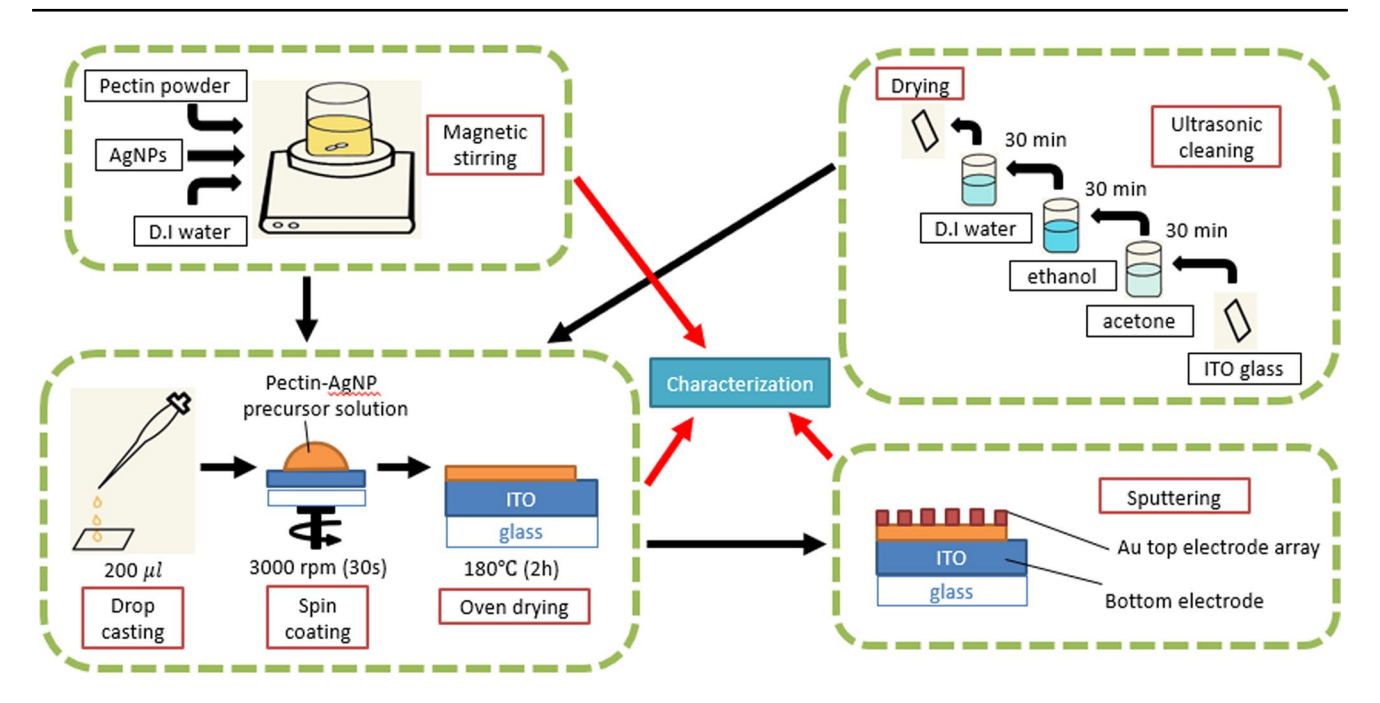


Fig. 2 Schematic of the experimental procedure for preparation of Au/pectin-AgNP/ITO devices.

a constant temperature of 180°C for 2 h in open air to dry the pectin-AgNP films. Once cooled to room temperature naturally within the oven, the samples were taken out and subjected to gold deposition via sputtering (Bio-Rad SEM Coating System E5100) to form an array of top electrodes on top of the solidified pectin-AgNP thin film using a metal shadow mask (Choon Automech, Penang, Malaysia). The resulting test structure was designated as Au/pectin-AgNP/ITO. Following the confirmation of the optimized AgNP concentration within the pectin, the second stage involved varying the concentrations of pectin while keeping the AgNP concentration constant.

The chemical functional groups present in the asreceived pectin powder, pectin-AgNP precursor solutions, and their solidified thin films were characterized using Fourier transform infrared (FTIR) spectroscopy (PerkinElmer Spectrum One). Prior to the measurement, a background scan was conducted using a blank ZnSe crystal window to offset any infrared absorption. The measurements were scanned eight times from 4000 cm<sup>-1</sup> to 400 cm<sup>-1</sup> with a resolution of 4 cm<sup>-1</sup>. The surface topography of the solidified pectin-AgNP thin films with a scanned area of 5 μm × 5 μm were characterized via atomic force microscopy (AFM) (SPA400 NanoNavi, Hitachi, Japan). Measurements were repeated on two different samples with the same parameters to obtain an average value. The average  $(R_a)$  and root-mean-square  $(R_{rms})$  surface roughness were computed using Gwyddion software (v2.62). The surface tension of the pectin-AgNP precursor solution and the static contact angle of the solution on the solidified surface of pectin-AgNP films were measured using a goniometer (Ramé-Hart 260, USA). All measurements were conducted under ambient conditions at room temperature with relative humidity of 40–55%. The pendant drop method was used for surface tension measurement, while the sessile drop method was used for contact angle measurement. The data were analyzed using DROPImage software version 2.7.0, and measurements for each sample were conducted in triplicate to obtain an average value.

The resistive switching characteristics of the test structures were measured using a Precision Semiconductor Parameter Analyzer (4156C, Agilent, Santa Clara, CA, USA) under ambient conditions. The samples were positioned on a probe station (PE-2, Everbeing Int'l Corp., Taiwan) with two mobile probing needles connected to the semiconductor parameter analyzer and controlled via Metrics ICS v3.6 software. The voltage was applied at the Au top electrode (TE), while the ITO bottom electrode (BE) was held at constant ground potential for all measurements. A compliance current of 0.1 A was maintained, and the DC voltage sweep rate was set at 0.1 V/s.



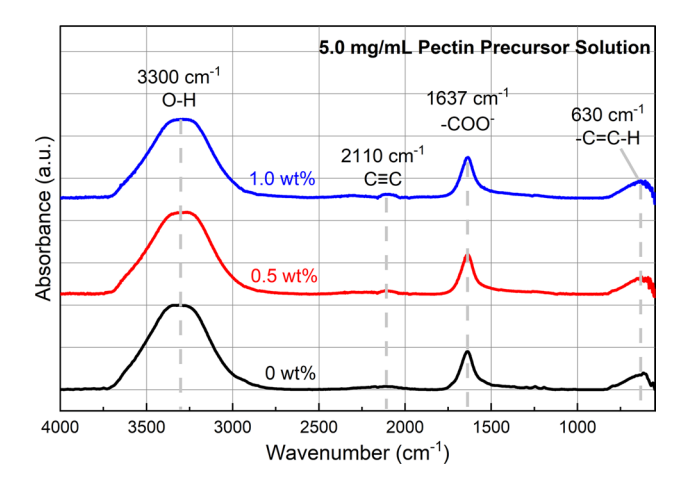


Fig. 3 FTIR spectra of 5.0 mg/mL pectin-polysaccharide precursor solution with different concentrations of AgNP (0.0 wt.%, 0.5 wt.%, and 1.0 wt.%).

#### **Results and Discussion**

# Effects of Different Silver Nanoparticle (AgNP) Concentrations

### **FTIR Analyses**

Figure 3 shows the FTIR spectra of 5.0 mg/mL pectin-AgNP precursor solution with different concentrations of AgNP (0.0 wt.%, 0.5 wt.%, and 1.0 wt.%). All samples revealed similar absorbance peaks at 3300 cm<sup>-1</sup>, 2110 cm<sup>-1</sup>, 1637 cm<sup>-1</sup>, and 630 cm<sup>-1</sup>, corresponding to chemical functional groups of −OH, C≡C, −COO<sup>-</sup>, and −C=C−H, respectively. These functional groups are associated with the pectin monomer, as shown in Fig. 1, except for C≡C. However, differences in the area under the respective peaks of 2110 cm<sup>-1</sup>, 1637 cm<sup>-1</sup>, and 630 cm<sup>-1</sup>, which represent the difference in the abundance of chemical functional groups, are observed and calculated. A notable change in the abundance of C≡C (2110 cm<sup>-1</sup>) (Fig. 4a), −COO<sup>-</sup> (1637 cm<sup>-1</sup>) (Fig. 4b) and −C=C−H (630 cm<sup>-1</sup>) (Fig. 4c) was recorded, correlating

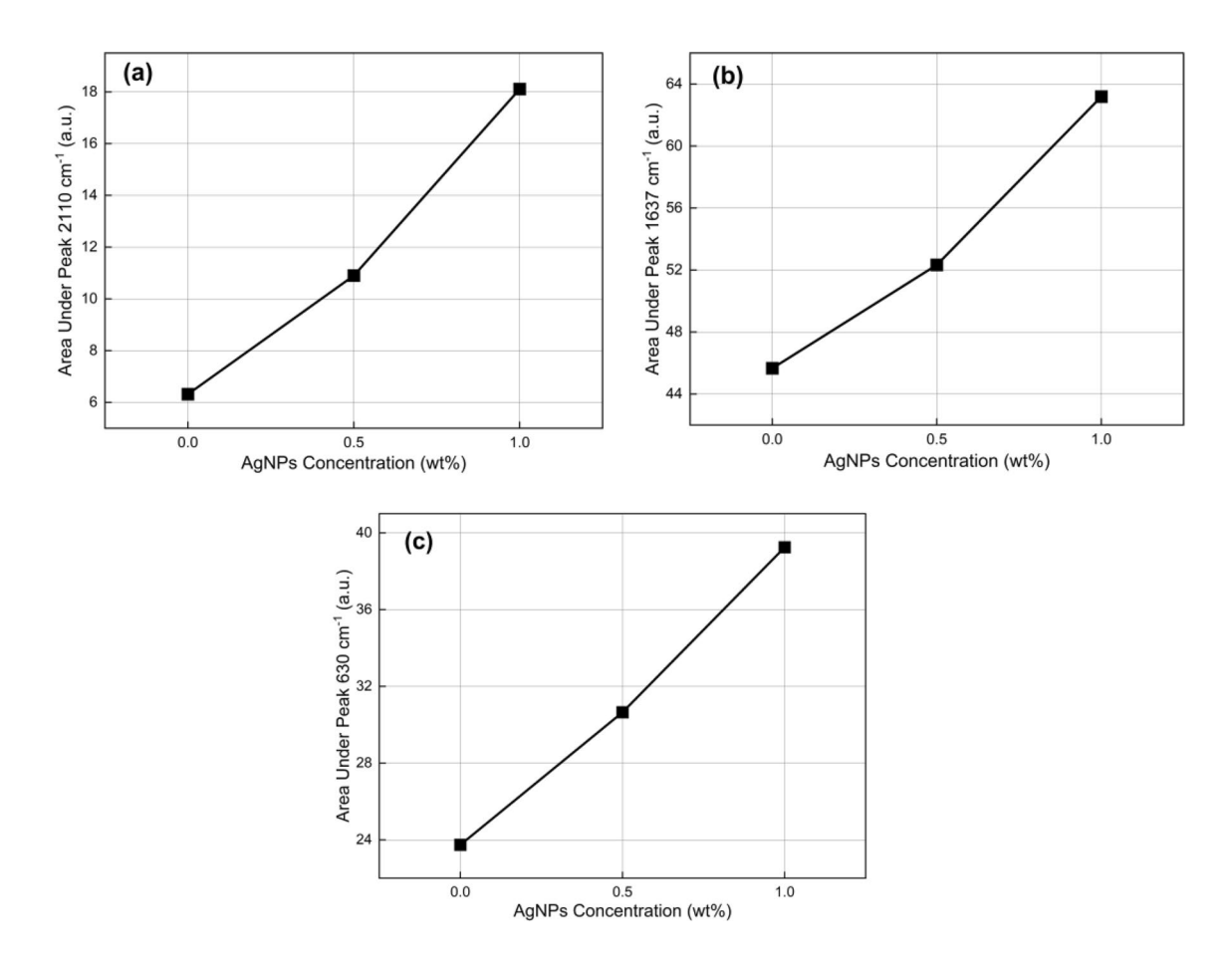


**Fig. 4** Areas under the (a) 2110, (b) 1637, and (c) 630 cm<sup>-1</sup> peaks from Fig. 3, representing vibration of C≡C, hydrolysis of –COOH, and stretching of aromatic C–H functional groups in the pectin-AgNP precursor solution as a function of AgNP concentration.



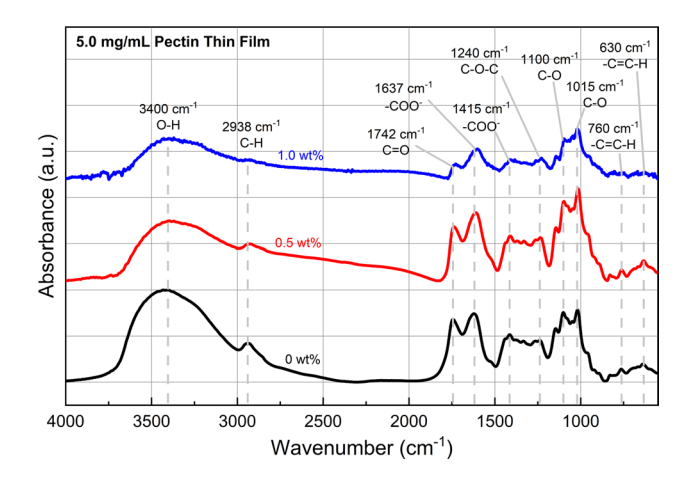
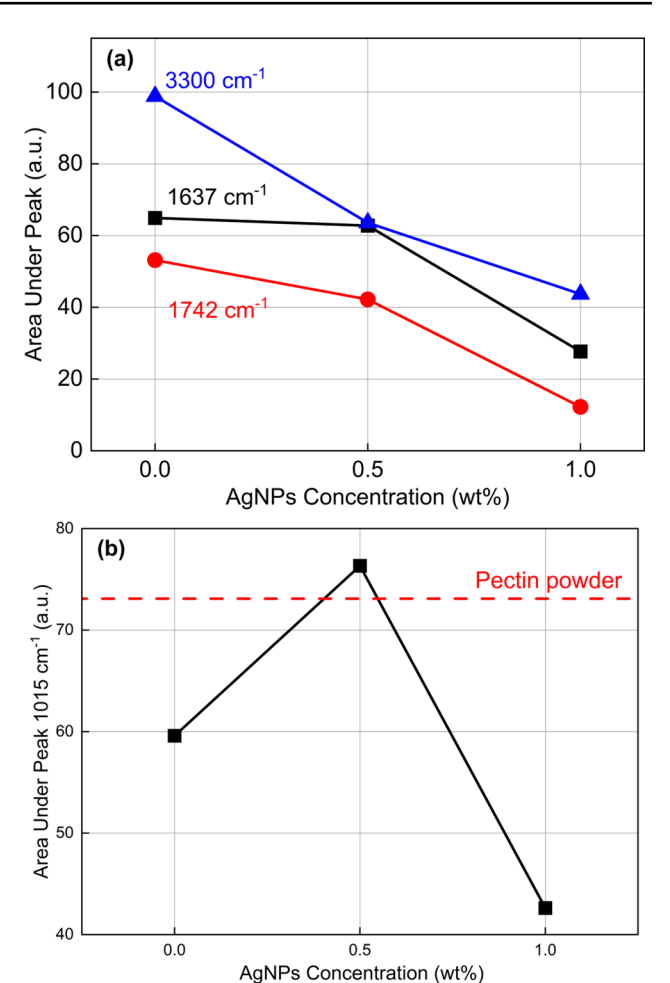


Fig. 5 FTIR spectra of pectin-AgNP thin films after drying at  $180\,^{\circ}$ C with different AgNP concentrations (0.0 wt.%, 0.5 wt.%, and 1.0 wt.%).

with the area under the respective absorbance peaks (Fig. 4). The presence of  $C \equiv C$  in the solution increases with AgNP concentration, indicating enhanced de-esterification and hydrolysis of pectin long chains into monomers, as this functional group is absent from the pectin monomer. At the same time, with the increase in AgNP concentration up to 1.0 wt.%, the presence of -COO<sup>-</sup> and -C=C-H continues to increase. These functional groups originate from the pectin monomer, and the increase in carboxylate ions is associated with the increase in AgNP concentration, suggesting the incorporation of AgNP in the carboxylate ion of pectin. This is further supported by the presence of both hydrophobic ester and hydrophilic carboxyl groups in pectin. The hydrophobic parts enable pectin absorption onto the AgNP surface, while the hydrophilic parts facilitate interaction with water molecules for stabilization.<sup>29,30</sup> Moreover, the abundance of hydroxyl (O-H) remained unchanged as a function of AgNP concentration, further indicating the incorporation of AgNP at the carboxylate site.

After the pectin-AgNP precursor solution was deposited onto the ITO substrates and dried at 180°C, the FTIR spectra of the samples were measured and are presented in Fig. 5. The results revealed similar peaks as reported in previous studies 1,18,27,28 at 3400 cm<sup>-1</sup> (O–H), 2938 cm<sup>-1</sup> (C–H), 1742 cm<sup>-1</sup> (C=O), 1637 cm<sup>-1</sup> (-COO<sup>-</sup>), 1415 cm<sup>-1</sup> (-COO<sup>-</sup>), 1240 cm<sup>-1</sup> (C–O-C), 1100 cm<sup>-1</sup> (C–O), 1015 cm<sup>-1</sup> (C–O), 760 cm<sup>-1</sup> (C=C-H), and 630 cm<sup>-1</sup> (C=C-H), respectively, but with different intensities. Further analysis of the FTIR spectra of dried thin films also reveals the incorporation of AgNP at the carboxylate ion of pectin after the drying process. This is evidenced by absorbance peaks at 3300 cm<sup>-1</sup> (O–H), 1742 cm<sup>-1</sup> (C=O), and 1637 cm<sup>-1</sup> (-COO<sup>-</sup>). The presence of O–H, C=O, and -COO<sup>-</sup> bonds decreases with increasing AgNP



**Fig. 6** Areas under the (a) 3300, 1742, and 1637 cm<sup>-1</sup> peaks which represent O–H, C=O, and –COO<sup>-</sup>, respectively, and (b) the peak of 1015 cm<sup>-1</sup> which represents C–O in pectin-AgNP thin films as a function of AgNP concentration extracted from Fig. 5.

concentrations, as shown in Fig. 6a. However, it is notable that the presence of the C–O bond at 1015 cm<sup>-1</sup> increases until the concentration of AgNP reaches 0.5 wt.%. The abundance of C–O bonds at this concentration also surpasses that found in pristine pectin powder. Beyond this concentration, the presence of the C–O bond decreases, as shown in Fig. 6b, suggesting that the incorporation of AgNP has reached its saturation point within the pectin matrix. This primary chemical function group is related to the observed trend in the read memory window and the ON/OFF ratio for the resistive switching characteristics that will be elaborated in the subsequent sections.

#### **Wettability Analyses**

Figure 7 presents the surface tension of pectin-AgNP precursor solutions and the contact angles of these solutions on ITO substrates as a function of AgNP concentration.



The surface tension increases as the AgNP concentration increases from  $43.51 \pm 2.67$  mN/m to  $61.53 \pm 1.81$  mN/m. The increase may be attributed to the decreasing distance between AgNP as the concentration increases, leading to a higher van der Waals force and subsequently increasing cohesive force and surface tension. The results align with the findings from FTIR spectra, supporting the incorporation of AgNP within the pectin matrix. Furthermore, contact angle measurements of pectin-AgNP precursor solutions with different AgNP concentrations deposited on ITO substrates demonstrate an increasing trend as a function of the AgNP concentration, suggesting a decrease in the wettability of pectin-AgNP precursor solutions on the ITO surface with higher AgNP concentrations. Nevertheless, all

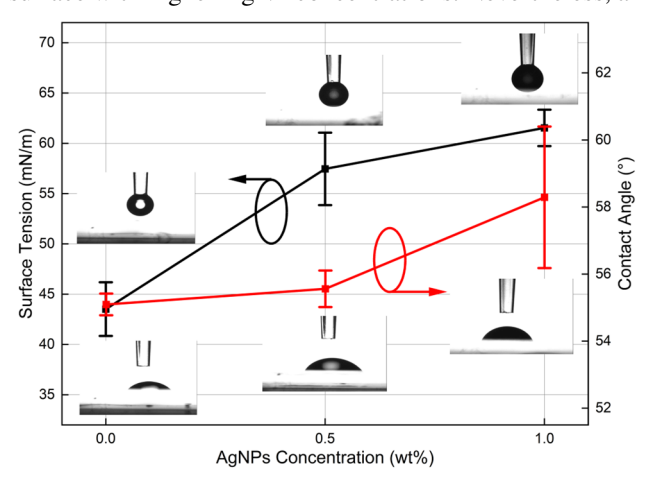


**Fig. 7** Surface tension (black curve) and contact angle (red curve) of pectin-AgNP precursor solution as a function of AgNP concentration on the ITO substrate (Color figure online).

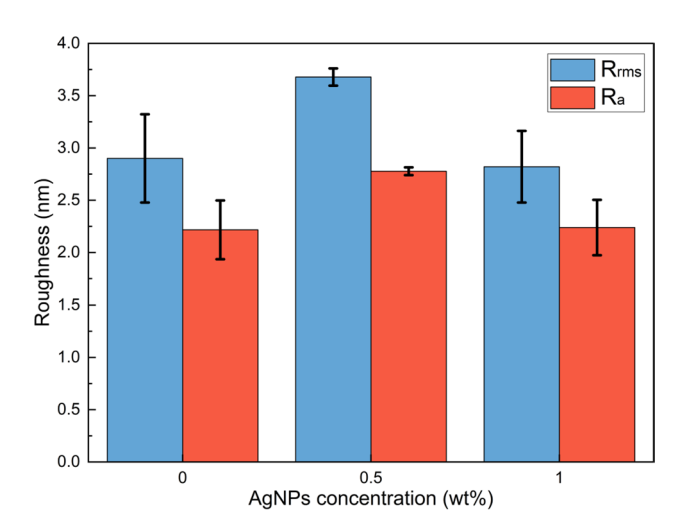


**Fig. 8** Average roughness  $(R_{\rm a})$  and root-mean-square roughness  $(R_{\rm rms})$  of the pectin-AgNP thin film surface with different AgNP concentrations.

recorded contact angles remained well below 90°, showing favourable spreading and adhesion of the solutions on the ITO surface.<sup>34</sup>

# **AFM Analyses**

Figure 8 presents a comparison of the average roughness ( $R_a$ ) and root-mean-square roughness ( $R_{rms}$ ) of the surface of the dried pectin-AgNP thin films with different AgNP concentrations examined by AFM. The trends show an increase in both  $R_a$  and  $R_{rms}$  values as a function of AgNP concentration, which aligns with the earlier findings on the incorporation of AgNP within the pectin matrix in Fig. 7. This incorporation leads to the formation of longer and more compacted branches of pectin molecules, thus increasing the stress in the pectin matrix and resulting in a higher value of surface roughness. Notably, beyond 0.5 wt.% AgNP concentration,  $R_a$  and  $R_{rms}$  values decrease, further supporting the conclusion drawn from the FTIR results (Figs. 5 and 6) that the solubility limit has been reached with the maximum amount of AgNP incorporated in the pectin matrix for this study.

Additionally, the increased surface roughness can be attributed to the increase in thin film thickness. As shown in Fig. 9, the bare pectin thin film had the lowest  $R_{\rm a}$  and  $R_{\rm rms}$  values, with thickness of approximately 950 nm, as reported in our previous work comparing the effects of different drying temperatures on pectin thin films. <sup>18</sup> In this study, the incorporation of AgNP within the pectin matrix led to the formation of longer and more compacted branches of pectin molecules, which likely resulted in increased film thickness compared to the previously measured thickness. The increased thickness of the pectin-AgNP thin film is related to

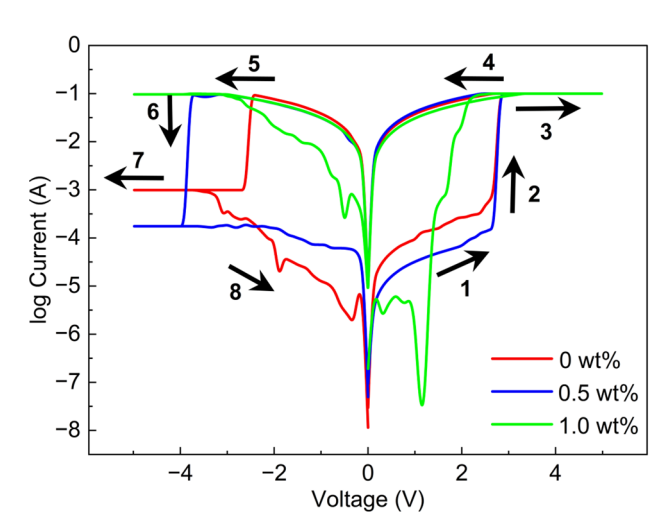


**Fig. 9** Current–voltage characteristics of pectin-AgNP-based memory with different AgNP concentrations of 0.0 wt.% (red curve), 0.5 wt.% (blue curve), and 1.0 wt.% (green curve). Sweeping direction and sequences are indicated by arrows and numbers (Color figure online).



the observed trend in the read memory window and the ON/ OFF ratio for the resistive switching characteristics, which will be elaborated in subsequent sections.

#### **Electrical Analyses**

Figure 9 presents the resistive switching characteristics of pectin-AgNP-based memory devices prepared with different AgNP concentrations. The results were smoothed using B-spline smoothing and anti-aliasing techniques in Origin 2024b software. All samples demonstrated a bipolar resistive switching mode, characterized by both SET and RESET processes occurring at voltages of opposite polarities. Notably, the sample with 1.0 wt.% AgNP did not exhibit a typical resistive switching behaviour. This observation aligns with the results of FTIR and AFM, indicating that the AgNP concentration reached maximum solubility within the pectin matrix, inhibiting the proper bipolar resistive switching characteristics. Meanwhile, for the other two samples, during positive voltage sweeping from 0 to +5 V (labelled "1"), the current progressively increased until an abrupt increased was observed (labelled "2"), indicating  $V_{\text{SET}}$  had been reached. Subsequently, the current remained stable as the voltage continued to sweep up to +5 V (labelled "3"). Upon voltage reversal from +5 V to 0 V and 0 V to -5 V, the current remained at a high level (labelled "4" and "5") until  $V_{\rm RESET}$ (labelled "6"), causing an instantaneous drop in the current. The current decreased progressively as the voltage swept to -5 V (labelled "7") before returning to its initial voltage (labelled "8"). As shown in Fig. 9, the high current levels labelled 3 to 5 represent the LRS, while the low current levels labelled 7, 8, and 1 indicate HRS in resistive switching memory. The difference in magnitude between  $V_{\rm SET}$  and  $V_{\text{RESET}}$  defines the read memory window. At a specific voltage, the ratio of current between LRS and HRS determines the ON/OFF ratio of the memory, while the specific voltage is defined as read voltage ( $V_{\rm READ}$ ), where data stored in the memory can be read.

Table II summarizes the  $V_{\rm SET}$ ,  $V_{\rm RESET}$ , read memory window, and ON/OFF ratio of the tested samples. The read memory window increases with increasing AgNP

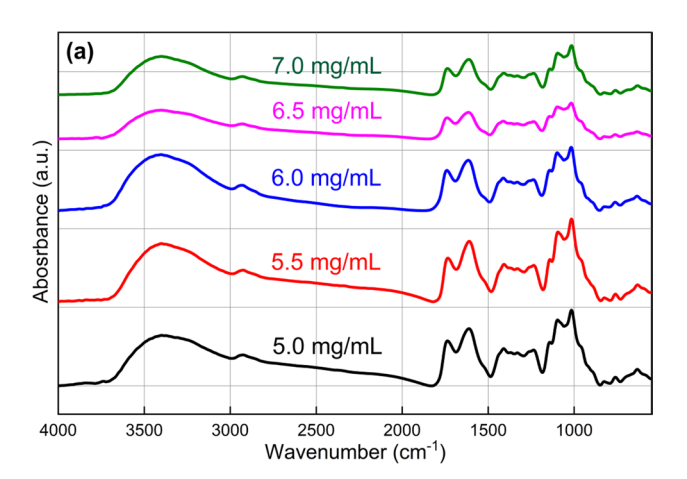
Table II  $V_{\rm SET}$ ,  $V_{\rm RESET}$ , read memory window, and ON/OFF ratio of pectin-AgNP-based memory devices as a function of AgNP concentration

AgNP concentration (wt.%)	V <sub>SET</sub> (V)	V <sub>RESET</sub> (V)	Read memory window (V)	ON/OFF ratio
0	2.7	-2.5	5.2	$3.6 \times 10^2$
0.5	2.7	-3.8	6.5	$1.3 \times 10^3$
1.0	N/C	N/C	N/C	N/C

N/C not countable



concentration up to 0.5 wt.%. These memory windows align with the reported values ranging from 1.5 V to 7.5 V for other bio-organic materials. 16,24,35-39 Additionally, ON/OFF ratios measured at  $V_{READ} = 0.1 \text{ V}$  are shown in Table II, with the values increasing until reaching a maximum at 0.5 wt.%. This trend mirrors the behaviour of C-O bonds in pectin-AgNP thin films [Fig. 6b]. The higher amounts of C-O bonds lead to higher incorporation of AgNP within the pectin matrix, forming longer and more compacted branches. This formation results in increased thin film thickness, and consequently, the resistance of the pectin-AgNP thin film is higher than that of the bare pectin thin film, contributing to a lower HRS value. Although a larger memory window implies higher power consumption, a high ON/OFF ratio is preferable for minimizing errors in differentiating resistance states during the reading of data while operating at lower energy levels. Therefore, the preference leans towards the higher ON/OFF ratio recorded with the AgNP concentration of 0.5 wt.%.



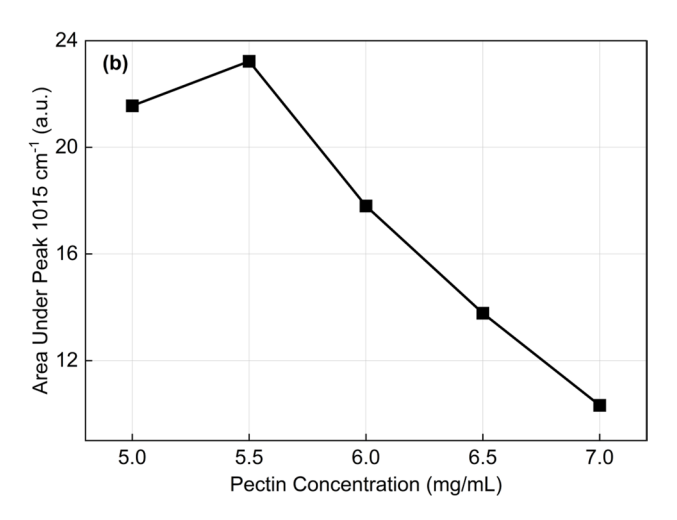


**Fig. 10** (a) FTIR spectra of pectin-AgNP thin films and (b) area under the peak at 1015 cm<sup>-1</sup> with different pectin concentrations from 5.0 mg/mL to 7.0 mg/mL.

#### **Effects of Different Pectin Concentrations**

#### **FTIR Analyses**

Given that AgNP exhibited maximum solubility within the pectin matrix at a concentration of 0.5 wt.%, the subsequent step involves investigating the effect of pectin concentrations (5.0 mg/mL, 5.5 mg/mL, 6.0 mg/mL, 6.5 mg/mL, and 7.0 mg/mL) with a fixed concentration of AgNP (0.5 wt.%). Figure 10a shows the FTIR spectra of pectin-AgNP thin films with different pectin concentrations, while Fig. 10b presents the area under the peak of 1015 cm<sup>-1</sup> for each pectin concentration. The results reveal that the presence of C-O bonds increases when the pectin concentration reaches 5.5 mg/mL, suggesting not only that a greater amount of AgNP has been incorporated within the pectin matrix but also that more linear and extended pectin chains were established by glycosidic bonds, as shown in Fig. 1. Nevertheless, beyond this concentration, the presence of the C-O bond decreased, indicating that the pectin reached its solubility limit after incorporating 0.5 wt.% AgNP. This primary chemical function group is related to the observed trend in the read memory window and the ON/OFF ratio for the resistive switching characteristics, which will be elaborated in the subsequent sections.

#### **Wettability Analyses**

Figure 11 presents the surface tension of the pectin-AgNP precursor solutions and the contact angles of these solutions

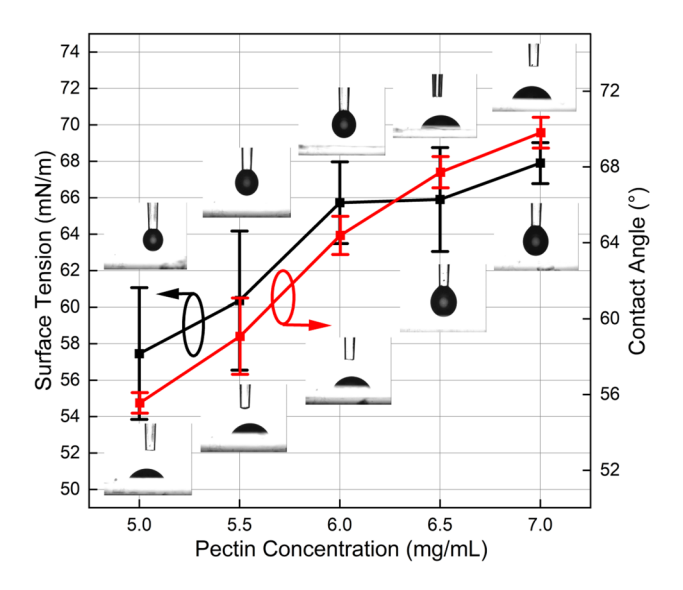
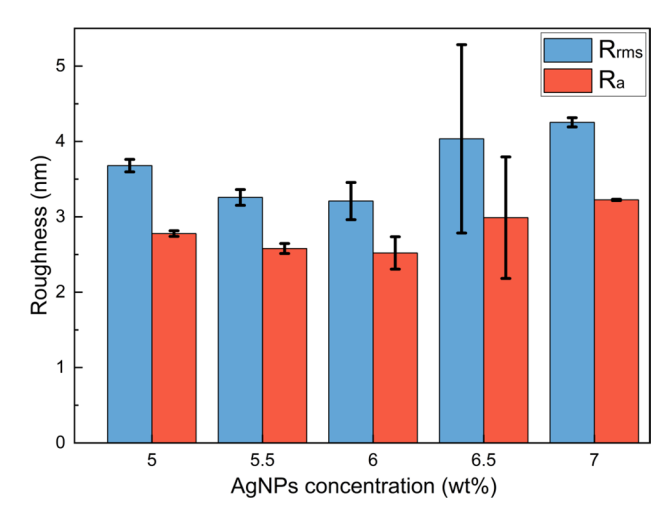


**Fig. 11** Surface tension (black curve) and contact angle (red curve) measurements of pectin-AgNP precursor solutions as a function of pectin concentration (Color figure online).

on ITO substrates as a function of pectin concentration. The surface tension measurements increase from  $57.46 \pm 3.61$  mN/m to  $67.9 \pm 1.123$  mN/m with pectin concentration. This increase is attributed to the decreasing distance between particles as the pectin concentration increases, leading to higher van der Waals forces and subsequently increasing cohesive force and surface tension.  $^{31-33}$  Furthermore, contact angle measurements of pectin-AgNP precursor solutions with different pectin concentrations deposited on ITO substrates indicate an increasing trend as a function of pectin concentration, suggesting a decrease in the wettability of pectin-AgNP precursor solutions on the ITO surface with higher pectin concentrations. Nevertheless, all recorded contact angles remained well below  $90^{\circ}$ , showing a favourable spreading and adhesion.  $^{34}$ 

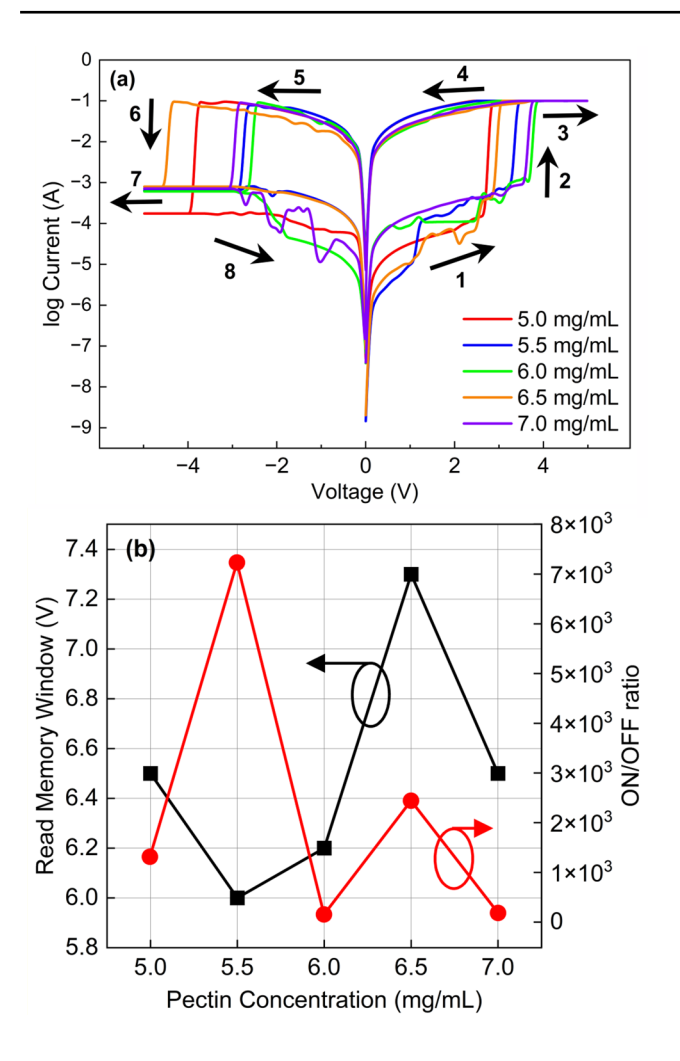
#### **AFM Analyses**

Figure 12 presents a comparison of the average roughness  $(R_{\rm a})$  and root-mean-square roughness  $(R_{\rm rms})$  of the surface of dried pectin-AgNP thin films with different pectin concentrations as examined by AFM. The comparison in Fig. 12 shows a decrease in both  $R_{\rm a}$  and  $R_{\rm rms}$  values as a function of pectin concentration. The trend in Fig. 12 contrasts with the trend observed in the presence of C–O bonds shown in Fig. 10b. These results suggest that a more uniform distribution of AgNP occurs at a lower pectin concentration, promoting the formation of C–O bonds that incorporate AgNP, thus reducing surface roughness. Beyond this concentration, where pectin has likely reached its maximum solubility, the distribution of AgNP within the pectin matrix is affected, leading to agglomeration, and subsequently increasing surface roughness. The non-uniform dispersion and particle



**Fig. 12** Average roughness  $(R_a)$  and root-mean-square roughness  $(R_{rms})$  of the pectin-AgNP thin film surface prepared at different pectin concentrations





**Fig. 13** (a) Current–voltage characteristics of pectin-AgNP-based memory with different pectin concentrations of 5.0 mg/mL (red curve), 5.5 mg/mL (blue curve), 6.0 mg/mL (red curve), 6.5 mg/mL (red curve), and 7.0 mg/mL (green curve). Sweeping direction and sequences are indicated by arrows and numbers. (b) Read memory window and ON/OFF ratio under these pectin concentrations (Color figure online).

agglomeration of AgNP at higher pectin matrix concentrations might result in unpredictable and inconsistent trends in thin film thickness, thereby adversely impacting the read memory window and the ON/OFF ratio for the resistive switching characteristics. These effects will be elaborated in subsequent sections.

#### **Electrical Analyses**

Figure 13a presents the resistive switching characteristics of pectin-AgNP-based memory devices prepared with different pectin concentrations. The results were smoothed using B-spline smoothing and anti-aliasing techniques in Origin 2024b software. All tested samples demonstrated a bipolar resistive switching mode. Figure 13b shows the read

memory window and ON/OFF ratio of the tested samples. The smallest read memory window was recorded from the sample with 5.5 mg/mL pectin concentration. Beyond this concentration, the read memory window increases. However, a decrease in the read memory window is observed in the sample with a 7.0 mg/mL pectin concentration, which may be attributed to the non-uniform dispersion and particle agglomeration of AgNP. This results in inconsistent film thickness and contributes to the observed variability in the read memory window. Additionally, the ON/OFF ratio measured at  $V_{READ} = 0.1 \text{ V}$  has the highest reading at a pectin concentration of 5.5 mg/mL among the pectin concentrations. This trend mirrors the behaviour of C-O bonds in pectin-AgNP thin films (Fig. 10b), where the presence of C–O bonds increases when the pectin concentration reaches 5.5 mg/mL. This increase indicates greater incorporation of AgNP within the pectin matrix and the formation of more linear and extended pectin chains established by glycosidic bonds. Beyond this concentration, the solubility limit of pectin was reached, resulting in a lower and inconsistent ON/ OFF ratio. This inconsistency is likely due to the variations in film thickness caused by the non-uniform dispersion and particle agglomeration of AgNP. Thus, the smallest read memory window and largest ON/OFF ratio are achievable with a 5.5 mg/mL pectin concentration together with a 0.5 wt.% AgNP concentration. This combination allows the device to minimize errors in differentiating resistance states during data reading while operating at lower energy levels.

# Proposed Mechanisms of Au/AgNP-Pectin/ITO ReRAM Device

The mechanisms of resistive switching behaviours of ReRAM are generally classified into three categories: electrochemical, electronic, and thermochemical. 13,40–44 Among these mechanisms, the electrochemical mechanism must meet two requirements to be considered the primary mechanism. First, the top electrode must be more reactive than the bottom electrode. Second, the memristive thin film must act as a medium to depolarize electrons from the top electrode but not from the bottom electrode. 41,44,45 Because the top electrode (Au) has a higher standard reduction potential than the bottom electrode (indium and tin) according to the standard electrode reduction potential series, the electrochemical mechanism does not apply to the pectin-AgNP-based memory device in this work. 46–49 Therefore, electronic and thermochemical mechanisms are proposed for the formation of conductive paths within the pectin film, assisted by silver nanoparticles. These two mechanisms are illustrated in Fig. 14.

The electronic mechanism involves the reversible transfer of carriers (electrons or holes) between electrodes via bulk bio-organic material. <sup>13,41,50</sup> Figure 14 presents



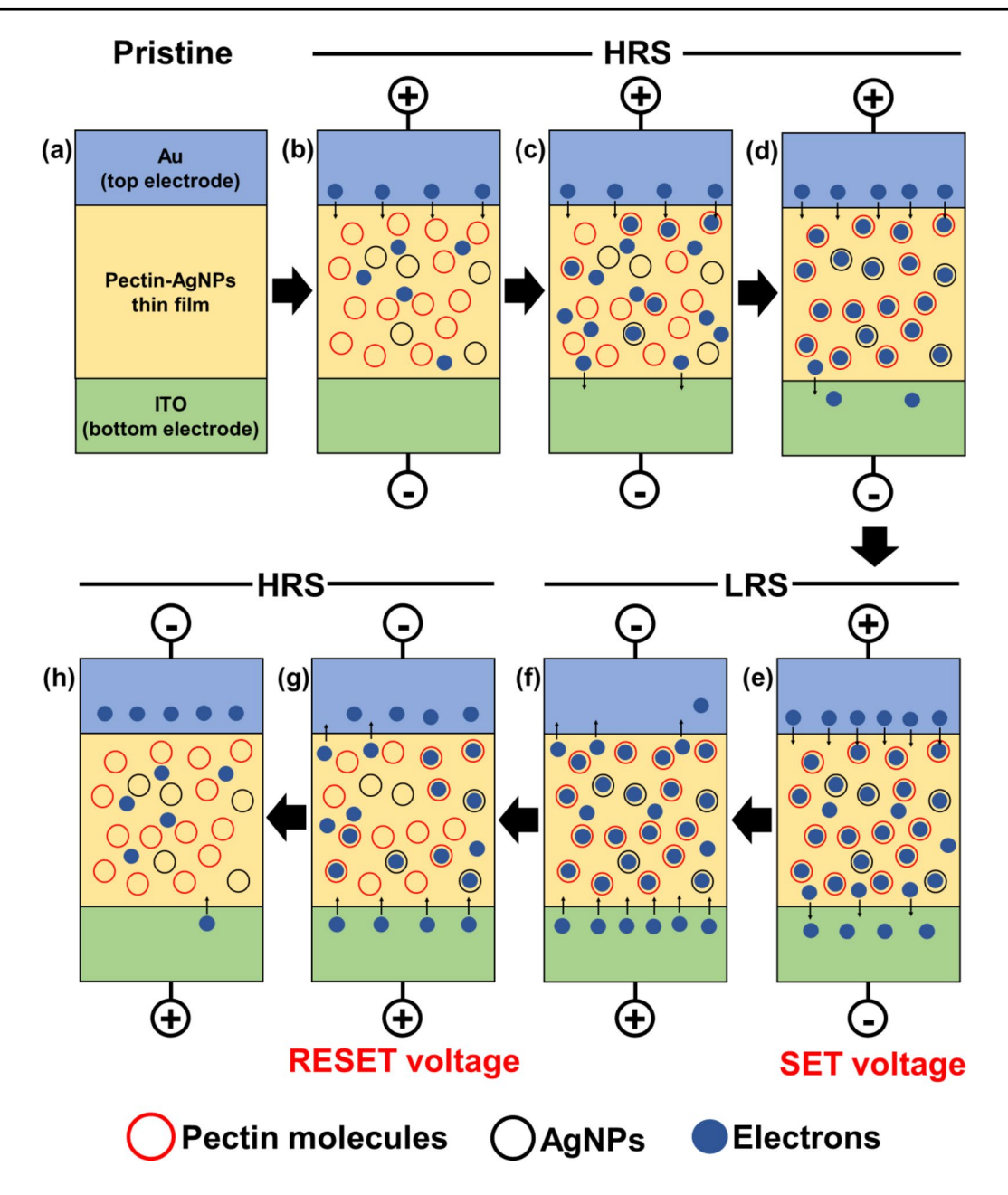


Fig. 14 Schematic of proposed resistive switching mechanisms for electronic conduction within the pectin-AgNP thin film

a schematic of the proposed electronic resistive switching mechanism within the pectin-AgNP thin film, which follows the sweeping direction and sequences of the *I–V* characteristics shown in Figs. 9 and 13a, respectively. Initially, the device was in HRS (Fig. 14a), attributed to the long pectin chain containing various pendant groups, as shown in Fig. 1, leading to a high defect density when the precursor transformed from a raw state to a solidified thin film. <sup>18,51</sup> When voltage is applied from the top electrode, the thin film experiences soft dielectric breakdown (Fig. 14b), and defects within the pectin matrix serve as active sites to trap and de-trap electrons (Fig. 14c). The

formation of active sites in the thin film can be attributed to the chemical structure of the pectin chains and the varying presence of C–O bonds, as shown in the FTIR spectra (Figs. 6b and 10b). Meanwhile, the presence of AgNP in the pristine metallic state (Ag<sup>0</sup>) transformed into the ionic state (Ag<sup>+</sup>) upon voltage application, as demonstrated in work by Yang et al. <sup>14</sup> and Wang et al. <sup>52</sup> This transformation indicates that AgNP contribute to increasing active sites for the trapping and de-trapping of electrons, thus further promoting electron transport and facilitating resistive switching.



As the voltage continues to increase, all the active sites, including both pectin and AgNP, are fully occupied, and space-charge-limited conduction (SCLC) occurs (Fig. 14d). Beyond SCLC, the current increases abruptly, and the device switches from HRS to LRS. This is because the concentration of electrons within the thin film is much lower than the concentration of injected electrons from the top electrode (Fig. 14e). The electrons move towards the bottom electrode freely without being trapped as voltage increases. LRS is maintained when the voltage is reversed from the bottom electrode to the top electrode (Fig. 14f) until it reaches the reset value (Fig. 14g), causing an instantaneous current drop and device switching back to HRS (Fig. 14h), in which the concentration of electrons within the thin film is higher than the concentration of the injected electrons from the bottom electrode.

Furthermore, regardless of the polarity, heat is generated and absorbed by the pectin-AgNP thin film due to the higher compliance current (0.1 A) used in this work relative to that in other studies, which have typically utilized a compliance current lower than 10 mA.<sup>5,39,52–56</sup> The absorbed thermal energy may cause pyrolysis in the pectin matrix, partially dissociating weakly bonded chemical compounds and altering the initial sp³ orbital of carbon into the sp² orbital, which has lower electrically resistive states <sup>13,40,44</sup> to facilitate the transport of electrons.

#### Conclusion

In summary, Au/pectin-AgNP/ITO ReRAM devices were fabricated and tested through structural, chemical, and electrical measurements to investigate the effects of the concentration of AgNP (0.0 wt.%, 0.5 wt.%, and 1.0 wt.%) and pectin (5.0 mg/mL, 5.5 mg/mL, 6.0 mg/mL, 6.5 mg/mL, and 7.0 mg/mL) on resistive switching characteristics. Notably, an AgNP concentration of 0.5 wt.% alongside a pectin concentration of 5.5 mg/mL revealed the highest presence of C–O bonds in the FTIR spectra, indicating the incorporation of AgNP at the carboxylate ion of pectin and the formation of more linear and extended pectin chains established by glycosidic bonds after the drying process. This abundance of C-O bonds results in the highest resistance of the pectin-AgNP thin film, leading to the most substantial ON/OFF ratio  $(7.2 \times 10^3)$  across all samples. Additionally, the resistive switching behaviours are governed by both electronic and thermochemical mechanisms. Electrons are trapped and de-trapped by the soft breakdown of the pectin thin film and AgNP, while joule heating is generated in the film due to a high compliance current applied. The results of this study highlight the potential of pectin-AgNP thin films as a promising candidate for resistive switching memory and the importance of precise control over AgNP and pectin concentrations in optimizing memory performance.

**Acknowledgments** K.Y.C. would like to acknowledge the financial support by the Universiti Sains Malaysia through Special Research University Grant (Individual) (1001.PBAHAN. 8014117). F. Z. acknowledges the support by the US National Science Foundation under Grants 2104976 and 2247342.

**Funding** Special Research University Grant (Individual), 1001.PBA-HAN. 8014117, Kuan Yew Cheong, National Science Foundation, 2104976, Feng Zhao, 2247342, Feng Zhao.

**Data Availability** The datasets analyzed during the current study are available from the corresponding author on reasonable request.

**Conflict of interest** The authors have no conflicts to disclose.

#### References

- M. Liu, Q. Yuan, B. Li, and Y. Sun, Multilevel logic operation and artificial synaptic plasticity based on pectin transient memristor. ACS Appl. Electron. Mater. 6(2), 1262–1273 (2024). https://doi. org/10.1021/acsaelm.3c01611.
- R. Waser, R. Dittmann, C. Staikov, and K. Szot, Redox-based resistive switching memories nanoionic mechanisms, prospects, and challenges. *Adv. Mater. (Deerfield Beach, Fla.)* 21(25–26), 2632 (2009). https://doi.org/10.1002/adma.200900375.
- B. Sun, G. Zhou, T. Guo, Y.N. Zhou, and Y.A. Wu, Biomemristors as the next generation bioelectronics. *Nano Energy* (2020). https:// doi.org/10.1016/j.nanoen.2020.104938.
- Y. Xiao, B. Jiang, Z. Zhang, S. Ke, Y. Jin, X. Wen, and C. Ye, A review of memristor: material and structure design, device performance, applications and prospects. *Sci. Technol. Adv. Mater.* (2023). https://doi.org/10.1080/14686996.2022.2162323.
- F.Y. Rahman, R. Deb, S. Sarkar, H. Banik, M.J. Uddin, S. Chakraborty, D. Bhattacharjee, and S.A. Hussain, Resistive switching behavior employing the ipomoea carnea plant for biodegradable rewritable read-only memory applications. ACS Appl. Electron. Mater. 5(7), 3685 (2023). https://doi.org/10.1021/acsae lm.3c00425.
- P. Tang, J. Chen, T. Qiu, H. Ning, X. Fu, M. Li, Z. Xu, D. Luo, R. Yao, and J. Peng, Recent advances in flexible resistive random access memory. *Appl. Syst. Innov.* (2022). https://doi.org/10.3390/ asi5050091.
- C. Wang, X. Li, Z. Sun, Y. Liu, Y. Yang, and L. Chen, Research progress in dielectric-layer material systems of memristors. *Inorganics (Basel)* 12(3), 87 (2024). https://doi.org/10.3390/inorganics12030087.
- T.S. Lebbie, O.D. Moyebi, K.A. Asante, J. Fobil, M.N. Brune-Drisse, W.A. Suk, P.D. Sly, J. Gorman, and D.O. Carpenter, E-waste in Africa: a serious threat to the health of children. *Int. J. Environ. Res. Public Health* (2021). https://doi.org/10.3390/ijerp h18168488.
- S.T. Ghulam and H. Abushammala, Challenges and opportunities in the management of electronic waste and its impact on human health and environment. *Sustainability* (2023). https://doi.org/10. 3390/su15031837.
- B. Moossa, H. Qiblawey, M.S. Nasser, M.A. Al-Ghouti, and A. Benamor, Electronic waste considerations in the Middle East and North African (MENA) region: a review. *Environ. Technol. Innov.* (2023). https://doi.org/10.1016/j.eti.2022.102961.



- L. Andeobu, S. Wibowo, and S. Grandhi, A systematic review of E-waste generation and environmental management of Asia Pacific countries. *Int. J. Environ. Res. Public Health* (2021). https://doi.org/10.3390/ijerph18179051.
- F.Y. Rahman, D. Bhattacharjee, and S.A. Hussain, An account of natural material-based nonvolatile memory device. *Proc. Natl. Acad. Sci. India Sect A: Phys. Sci.* (2023). https://doi.org/ 10.1007/s40010-023-00830-2.
- K.Y. Cheong, I.A. Tayeb, F. Zhao, and J.M. Abdullah, Review on resistive switching mechanisms of bio-organic thin film for non-volatile memory application. *Nanotechnol. Rev.* (2021). https://doi.org/10.1515/ntrev-2021-0047.
- C.-C. Yang, Y.-T. Tsai, H.-L. Hsu, S.-P. Chang, and Y.-K. Su, Silver-doped citrus pectin resistive random access memory with multilevel characteristics. ECS J. Solid-State Sci. Technol. 11(5), 055003 (2022). https://doi.org/10.1149/2162-8777/ ac67af.
- N. Ardjoum, S. Shankar, N. Chibani, S. Salmieri, and M. Lacroix, In situ synthesis of silver nanoparticles in pectin matrix using gamma irradiation for the preparation of antibacterial pectin/silver nanoparticles composite films. *Food Hydrocoll* (2021). https://doi. org/10.1016/j.foodhyd.2021.107000.
- J. Xu, X. Zhao, Z. Wang, H. Xu, J. Hu, J. Ma, and Y. Liu, Bio-degradable natural pectin-based flexible multilevel resistive switching memory for transient electronics. *Small* 15(4), 1803970 (2019). https://doi.org/10.1002/SMLL.201803970.
- H. Wang, J. Shi, J. Zhang, Z. Tao, H. Wang, Q. Yang, P.A. van Aken, and R. Chen, Pectin-assisted one-pot synthesis of MoS<sub>2</sub> nanocomposites for resistive switching memory application. *Nanoscale* 14(33), 12129–12135 (2022). https://doi.org/10.1039/ d2nr02558b.
- P.L. Yap, K.Y. Cheong, H.L. Lee, and F. Zhao, Effects of drying temperature on preparation of pectin polysaccharide thin film for resistive switching memory. *J. Mater. Sci. Mater. Electron.* 33(25), 19805–19826 (2022). https://doi.org/10.1007/s10854-022-08795-5.
- C. De Silva, N.M. Nawawi, M.M.A. Karim, S.A. Gani, M.J. Masarudin, B. Gunasekaran, and S.A. Ahmad, The mechanistic action of biosynthesised silver nanoparticles and its application in aquaculture and livestock industries. *Animals* (2021). https:// doi.org/10.3390/ani11072097.
- A. Naganthran, G. Verasoundarapandian, F.E. Khalid, M.J. Masarudin, A. Zulkharnain, N.M. Nawawi, M. Karim, C.A.C. Abdullah, and S.A. Ahmad, Synthesis, characterization and biomedical application of silver nanoparticles. *Materials* (2022). https://doi.org/10.3390/ma15020427.
- Q. Lin, S. Hao, W. Hu, M. Wang, Z. Zang, L. Zhu, J. Du, and X. Tang, Human hair keratin for physically transient resistive switching memory devices. *J Mater Chem C Mater* 7(11), 3315–3321 (2019). https://doi.org/10.1039/c8tc05334k.
- K. Nathanael, P. Pico, N.M. Kovalchuk, A.D. Lavino, M.J.H. Simmons, and O.K. Matar, Computational modelling and microfluidics as emerging approaches to synthesis of silver nanoparticles: a review. *Chem. Eng. J.* (2022). https://doi.org/10.1016/j.cej.2022. 135178.
- L. Xu, Y.Y. Wang, J. Huang, C.Y. Chen, Z.X. Wang, and H. Xie, Silver nanoparticles: synthesis, medical applications and biosafety. *Theranostics* (2020). https://doi.org/10.7150/thno. 45413
- B. Sun, X. Zhang, G. Zhou, P. Li, Y. Zhang, H. Wang, Y. Xia, and Y. Zhao, An organic nonvolatile resistive switching memory device fabricated with natural pectin from fruit peel. *Org. Electron.* 42, 181–186 (2017). https://doi.org/10.1016/j.orgel.2016.12.037.
- 25. X. Wang, S. Tian, B. Sun, X. Li, B. Guo, Y. Zeng, B. Li, and W. Luo, From natural biomaterials to environment-friendly and

- sustainable nonvolatile memory device. *Chem. Phys.* 513, 7–12 (2018). https://doi.org/10.1016/j.chemphys.2018.06.013.
- M.S. Abbasi, M.S. Irshad, N. Arshad, I. Ahmed, M. Idrees, S. Ahmad, Z. Wei, M. Sharaf, and M.D. Al Firdausi, Biomaterial-induced stable resistive switching mechanism in TiO<sub>2</sub> thin films: the role of active interstitial sites/ions in minimum current leakage and superior bioactivity. ACS Omega 5(30), 19050 (2020). https://doi.org/10.1021/acsomega.0c02410.
- N. Arshad, M.S. Irshad, M.S. Abbasi, S. Ur Rehman, I. Ahmed, M.Q. Javed, S. Ahmad, M. Sharaf, and M.D. Al Firdausi, Green thin film for stable electrical switching in a low-cost washable memory device: proof of concept. RSC Adv. 11(8), 4327 (2021). https://doi.org/10.1039/d0ra08784j.
- K.-W. Lin, T.-Y. Wang, and Y.-C. Chang, Impact of top electrodes on the nonvolatile resistive switching properties of citrus thin films. *Polymers* (2021). https://doi.org/10.3390/polym13050710.
- N.S. Said, I.F. Olawuyi, and W.Y. Lee, Pectin hydrogels: gel-forming behaviors, mechanisms, and food applications. *Gels* (2023). https://doi.org/10.3390/gels9090732.
- J. Dolinska, M. Holdynski, P. Pieta, W. Lisowski, T. Ratajczyk, B. Palys, A. Jablonska, and M. Opallo, Noble metal nanoparticles in pectin matrix. preparation, film formation, property analysis, and application in electrocatalysis. ACS Omega 5(37), 23909–23918 (2020). https://doi.org/10.1021/acsomega.0c03167.
- K. Hileuskaya, A. Ladutska, V. Kulikouskaya, A. Kraskouski, G. Novik, I. Kozerozhets, A. Kozlovskiy, and V. Agabekov, "Green' approach for obtaining stable pectin-capped silver nanoparticles: physico-chemical characterization and antibacterial activity. Colloids Surf A Physicochem Eng Asp (2020). https://doi.org/10.1016/j.colsurfa.2019.124141.
- V.G.L. Souza, I.P. Mello, O. Khalid, J.R.A. Pires, C. Rodrigues, M.M. Alves, C. Santos, A.L. Fernando, and I. Coelhoso, Strategies to improve the barrier and mechanical properties of pectin films for food packaging: comparing nanocomposites with bilayers. *Coatings* (2022). https://doi.org/10.3390/coatings12020108.
- S. Tanvir, and L. Qiao, Surface tension of nanofluid-type fuels containing suspended nanomaterials. *Nanoscale Res. Lett.* (2012). https://doi.org/10.1186/1556-276X-7-226.
- M. Hammi, Surface and interface investigations of matrix-fillers in heterogeneous amorphous semiconductors. ACS Omega 6(49), 34075–34085 (2021). https://doi.org/10.1021/acsomega.1c05314.
- Y. Kim, J.S. An, D. Lee, S.Y. Ryu, Y.C. Hwang, D.H. Kim, and T.W. Kim, Biocompatible memristive device based on an agarose@gold nanoparticle-nanocomposite layer obtained from nature for neuromorphic computing. *Sci. Rep.* 13(1), 6491 (2023). https://doi.org/10.1038/s41598-023-32860-6.
- N. He, Y. Sun, Q. Yuan, Y. Wang, and S. Zuo, Biodegradable natural chitosan coating films-based flexible resistive switching memory for transient electronics. *Mater Sci Eng B Solid State Mater Adv Technol* (2023). https://doi.org/10.1016/j.mseb.2023. 116578.
- M. Saha, S.M. Nawaz, B.K. Keshari, and A. Mallik, Natural-casein-based biomemristor with pinched current-voltage characteristics. ACS Appl. Bio Mater. 5(2), 833 (2022). https://doi.org/10.1021/acsabm.1c01188.
- Y. Xing, B. Sueoka, K.Y. Cheong, and F. Zhao, Nonvolatile resistive switching memory based on monosaccharide fructose film. *Appl. Phys. Lett.* (2021). https://doi.org/10.1063/5.0067453.
- L. Wang, Y. Zhang, P. Zhang, and D. Wen, Physically transient, flexible, and resistive random access memory based on silver ions and egg albumen composites. *Nanomaterials* (2022). https://doi. org/10.3390/nano12173061.
- Z. Shen, C. Zhao, Y. Qi, W. Xu, Y. Liu, I.Z. Mitrovic, L. Yang, and C. Zhao, Advances of RRAM devices: Resistive switching mechanisms, materials and bionic synaptic application. *Nanomaterials* (2020). https://doi.org/10.3390/nano10081437.



- F. Zahoor, F.A. Hussin, U.B. Isyaku, S. Gupta, F.A. Khanday, A. Chattopadhyay, and H. Abbas, Resistive random access memory: introduction to device mechanism, materials and application to neuromorphic computing. *Discover Nano* (2023). https://doi.org/10.1186/s11671-023-03775-y.
- 42. V. Gupta, S. Kapur, S. Saurabh, and A. Grover, Resistive random access memory: a review of device challenges. *IETE Tech. Rev.* 37(4), 377 (2020). https://doi.org/10.1080/02564602.2019.16293
- C.C. Hsu, P.T. Liu, K.J. Gan, D.B. Ruan, and S.M. Sze, Oxygen concentration effect on conductive bridge random access memory of InWZnO thin film. *Nanomaterials* (2021). https://doi.org/10. 3390/nano11092204.
- S.S. Kundale, G.U. Kamble, P.P. Patil, S.L. Patil, K.A. Rokade, A.C. Khot, K.A. Nirmal, R.K. Kamat, K.H. Kim, H.M. An, T.D. Dongale, and T.G. Kim, Review of electrochemically synthesized resistive switching devices: memory storage, neuromorphic computing, and sensing applications. *Nanomaterials* (2023). https:// doi.org/10.3390/nano13121879.
- I. Valov, Interfacial interactions and their impact on redox-based resistive switching memories (ReRAMs). *Semiconductor Sci. Technol.* 32(9), 093006 (2017). https://doi.org/10.1088/1361-6641/aa78cd.
- S. Chen, L. Wang, Q. Zhang, and J. Liu, Liquid metal fractals induced by synergistic oxidation. *Sci Bull (Beijing)* 63(22), 1513– 1520 (2018). https://doi.org/10.1016/j.scib.2018.10.008.
- B.R. Karimadom, and H. Kornweitz, Mechanism of producing metallic nanoparticles, with an emphasis on silver and gold nanoparticles, using bottom-up methods. *Molecules* (2021). https://doi. org/10.3390/molecules26102968.
- L. Rocchetti, A. Amato, and F. Beolchini, Recovery of indium from liquid crystal displays. *J. Clean. Prod.* 116, 299 (2016). https://doi.org/10.1016/j.jclepro.2015.12.080.
- P. Mayer, and R. Holze, Electrocatalysis of redox reactions by metal nanoparticles on graphite electrodes. *J. Solid State Electrochem.* 5(6), 402 (2001). https://doi.org/10.1007/s100080000169.
- Y.C. Shen, C.Y. Chen, L. Lee, C.H. Chiang, Y.C. Hsu, R.H. Cyu, Y.R. Peng, Y.J. Yu, H.C. Kuo, T.Y. Tseng, and Y.L. Chueh, Twodimensional (2D) materials-inserted conductive bridge random

- access memory: controllable injection of cations in vertical stacking alignment of MoSe<sub>2</sub> layers prepared by plasma-assisted chemical vapor reaction. *ACS Mater Lett* 5(5), 1401–1410 (2023). https://doi.org/10.1021/acsmaterialslett.3c00013.
- V. Chandel, D. Biswas, S. Roy, D. Vaidya, A. Verma, and A. Gupta, Current advancements in pectin: extraction, properties and multifunctional applications. Foods (2022). https://doi.org/10.3390/foods11172683.
- Q. Wang, Y. Deng, J. Chen, L. Lu, Y. Ma, and L. Zang, Electrochemical preparation of polypyrrole-Ag nanoparticles composite film and its resistive switching properties. *J. Alloys Compd.* (2022). https://doi.org/10.1016/j.jallcom.2022.167117.
- X. Xiao, J. Guo, Z. Gao, D. Zhai, R. Liu, S. Qin, M.K. Alam, and Z. Sun, "Understanding the complementary resistive switching in egg albumen-based single sandwich structure with non-inert Al electrode. *Mater Res Express* (2023). https://doi.org/10.1088/ 2053-1591/acd67d.
- Z.W. Dlamini, S. Vallabhapurapu, and V.S. Vallabhapurapu, Resistive switching property of raw organic cow milk for memory application. *Sustainability (Switzerland)* (2023). https://doi.org/ 10.3390/su15108250.
- Y. Guo, W. Hu, F. Zeng, C. Zhang, Y. Peng, and Y. Guo, Ultrafast degradable resistive switching memory based on α-lactose thin films. *Org. Electron.* (2020). https://doi.org/10.1016/j.orgel.2020. 105750.
- M. Saha, S. Dey, S.M. Nawaz, and A. Mallik, Environmentfriendly resistive memory based on natural casein: role of electrode and bio-material concentration. *Org. Electron.* (2023). https://doi.org/10.1016/j.orgel.2023.106869.

**Publisher's Note** Springer Nature remains neutral with regard to jurisdictional claims in published maps and institutional affiliations.

Springer Nature or its licensor (e.g. a society or other partner) holds exclusive rights to this article under a publishing agreement with the author(s) or other rightsholder(s); author self-archiving of the accepted manuscript version of this article is solely governed by the terms of such publishing agreement and applicable law.

#### **Authors and Affiliations**

Jia Zheng Yeoh<sup>1</sup> · Muhammad Awais<sup>1</sup> · Feng Zhao<sup>2</sup> · Kuan Yew Cheong<sup>1</sup>

- ⊠ Kuan Yew Cheong srcheong@usm.my
- Electronic Materials Research Group, School of Materials and Mineral Resources Engineering, Engineering Campus, Universiti Sains Malaysia, 14300 Nibong Tebal, Seberang Perai Selatan, Pulau Pinang, Malaysia
- Micro/Nanoelectronic and Energy Laboratory, School of Engineering and Computer Science, Washington State University, Vancouver, WA 98686, USA

